ELSEVIER

Journal of Structural Geology 26 (2004) 1707–1725

JOURNAL OF STRUCTURAL GEOLOGY

www.elsevier.com/locate/jsg

Patterns of fault displacement and strain at Yucca Mountain, Nevada

Alan P. Morris[a,*], David A. Ferrill[b], Darrell W. Sims[b], Nathan Franklin[b], Deborah J. Waiting[b]

[a]*Department of Earth and Environmental Science, University of Texas at San Antonio, San Antonio, TX 78249, USA*
[b]*CNWRA, Southwest Research Institute®, San Antonio, TX 78238-5166, USA*

Received 1 November 2002; received in revised form 5 December 2003; accepted 5 December 2003

Abstract

Yucca Mountain, Nevada, is the sole candidate site for underground disposal of high-level radioactive waste in the United States. The mountain is composed of Tertiary (12.8–11.6 Ma) volcanic tuff, cut by west-dipping normal faults that divide the mountain into north-trending, east-dipping cuestas. Geologic characterization of Yucca Mountain by the U.S. Department of Energy (DOE) has focused on mapping lithostratigraphic units, faults (including single plane, small-displacement surfaces of discontinuity, and large-displacement fault zones), and fractures (quasi-planar zones that have experienced loss of cohesion, including joints, partially mineralized joints, veins, and small-displacement faults). Faults and fractures are important to repository design because they affect seismic hazard, rockfall, and fluid transmissivity in the surrounding rock mass. Geologic maps and detailed studies of rock pavements and tunnel walls reveal that faults and fractures within Yucca Mountain are not uniform in orientation or intensity. We investigate two aspects of distributed deformation arising from fault displacement patterns at Yucca Mountain. First, fault-parallel strains (elongation parallel to cutoff lines where stratigraphic horizons intersect fault planes) develop as a result of lateral fault displacement gradients. Using existing data, we analyze the likely state of strain in fault blocks at Yucca Mountain. Second, fault-strike-perpendicular strains can develop where two normal faults propagate past each other. A component of the total strain is distributed into the surrounding rock to produce synthetic layer dip or a network of smaller faults and fractures. We find that small-scale faulting and fracturing at Yucca Mountain is variable and is strongly controlled by larger scale fault system architecture.

Keywords: Normal faults; Displacement; Strain distribution; Yucca Mountain

1. Introduction

Yucca Mountain, Nevada is located within the southwestern part of the Basin and Range province, on the eastern margin of the Walker Lane Belt (Fig. 1a). It is the proposed site for the permanent disposal of high-level radioactive waste in the United States. The region is experiencing strike-slip and extensional deformation that has been active since the beginning of the Cenozoic (65 Ma) (see, for example, Snow and Wernicke, 2000). The region remains tectonically active as indicated by evidence for Quaternary (including Holocene) to present-day faulting (Harmsen, 1994; Simonds et al., 1995; Ferrill et al., 1996a,b), and Quaternary volcanism (Connor and Hill, 1995; Connor et al., 2000). Yucca Mountain itself is composed of faulted and fractured Miocene volcanic tuffs erupted from calderas in the Southwest Nevada Volcanic Field 15 to 9 million years ago, and deposited primarily as pyroclastic flow and ash fall deposits (Byers et al., 1976; Sawyer et al., 1994; Buesch and Spengler, 1998; Potter et al., 2002). The Tiva Canyon Tuff (12.7 Ma) of the Paintbrush Group makes up the main surface exposures of Yucca Mountain. The proposed repository would be hosted within the Topopah Spring Tuff (12.8 Ma), also of the Paintbrush Group. Angular unconformities and fault-related depocenters within the tuff sequence at Yucca Mountain indicate that faulting and tuff deposition occurred over the same period of time, and some volcanic and fault slip events may have been simultaneous and genetically linked (e.g. Carr, 1990; Day et al., 1998b; Fridrich, 1999; Dunne et al., 2003). Most faults at Yucca Mountain are either north-trending normal faults or northwest-trending, dextral strike-slip faults. The larger faults in these two orientations bound the fault blocks of Yucca Mountain (e.g. the Abandoned Wash, Solitario Canyon, Fatigue Wash, Northern Windy Wash, and Drill Hole Wash

* Corresponding author. Tel.: +1-210-458-4455; fax: +1-210-458-4469.
E-mail address: alanm52@flash.net (A.P. Morris).

0191-8141/$ - see front matter © 2004 Elsevier Ltd. All rights reserved.
doi:10.1016/j.jsg.2003.12.005

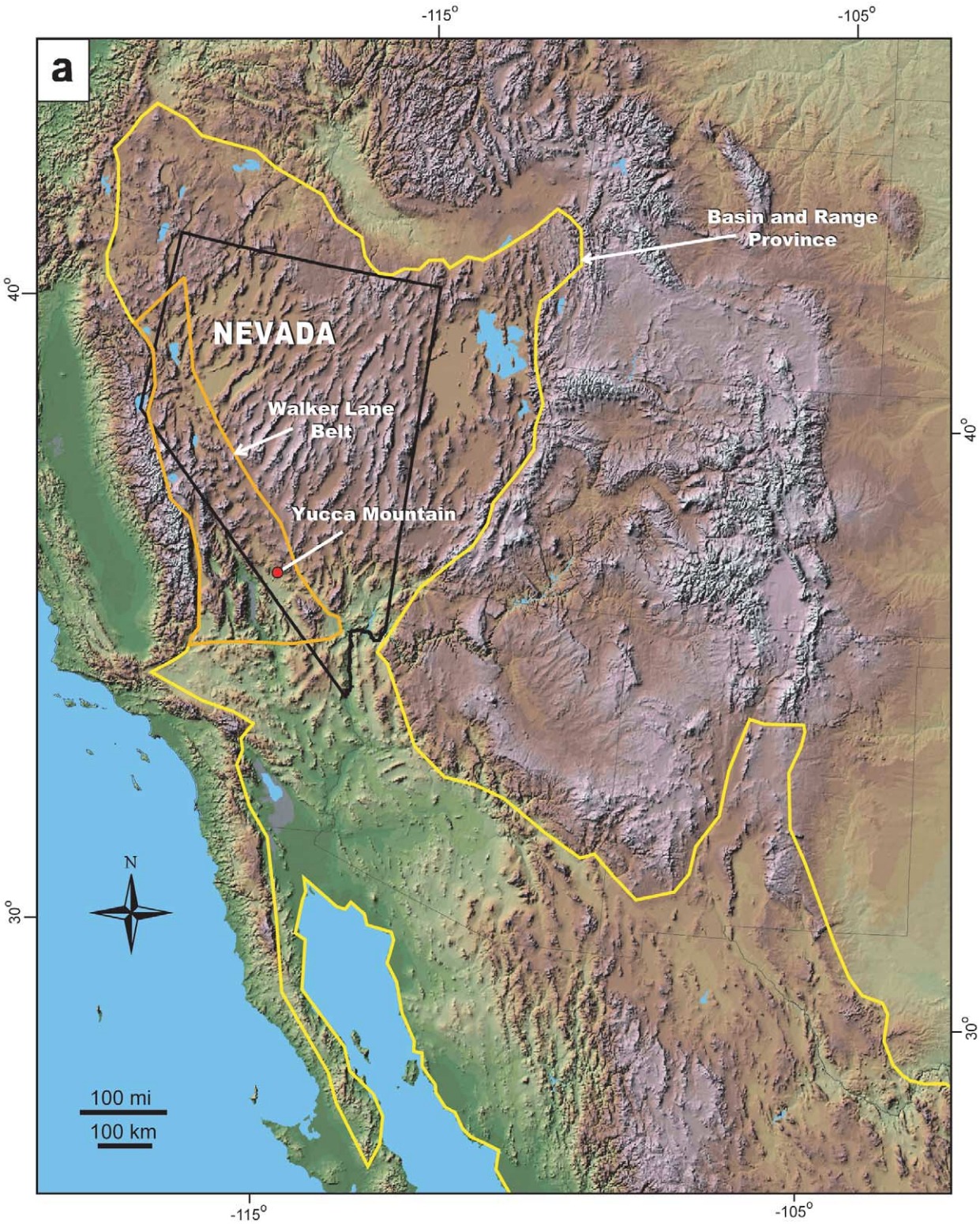

Fig. 1. (a) Shaded relief map (from U.S. Geological Survey, 1999) showing location of Yucca Mountain within Walker Lane and Basin and Range physiographic province (after Twiss and Moores, 1992; figure 1 in Oldow, 1992). (b) Location map of Yucca Mountain illustrating mapped faults (black lines) (Day et al., 1998a), and the surface projections of the two tunnels (red lines): Exploratory Studies Facility (ESF), and the Enhanced Characterization of the Repository block (ECRB). Background is an Ikonos-2 image from Space Imaging.

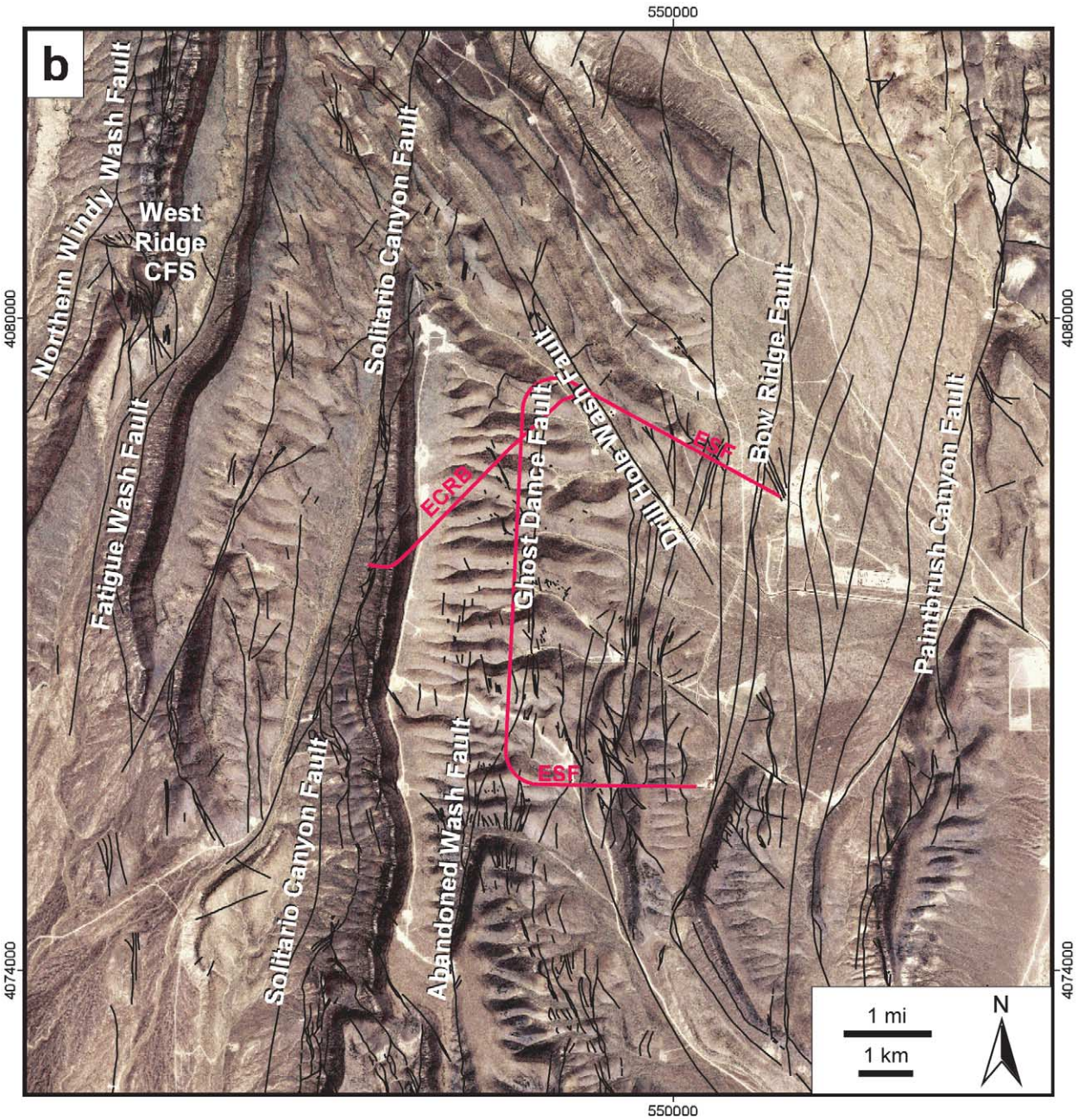

Fig. 1 (*continued*)

faults; Fig. 1b). Some northwest-trending faults are normal faults, accommodating extension in relay ramps between overlapping normal faults (Ferrill et al., 1999a).

Faults are defined here to include single plane, small-displacement surfaces of discontinuity, and large-displacement fault zones. We define fractures as quasi-planar zones that have experienced loss of cohesion, including joints, partially mineralized joints, veins, and small-displacement faults. The fault and fracture framework of Yucca Mountain and its environs are important to technical considerations with respect to the location, design, and long-term performance of the proposed waste repository. The United States Department of Energy (DOE) has responsibility for characterizing Yucca Mountain as a proposed high-level radioactive waste repository site, and the design of the proposed repository. Faults and fractures provide potential pathways for fluid movement, and bound blocks of rock that may fall from the walls and ceiling of excavated waste emplacement drifts. Therefore, the fault and fracture framework is a key factor in repository design and performance. Thus far, detailed fault and fracture characterization at Yucca Mountain has concentrated on an area between the Solitario Canyon and Bow Ridge faults (Fig. 1b; CRWMS M&O, 2001). These two faults have maximum

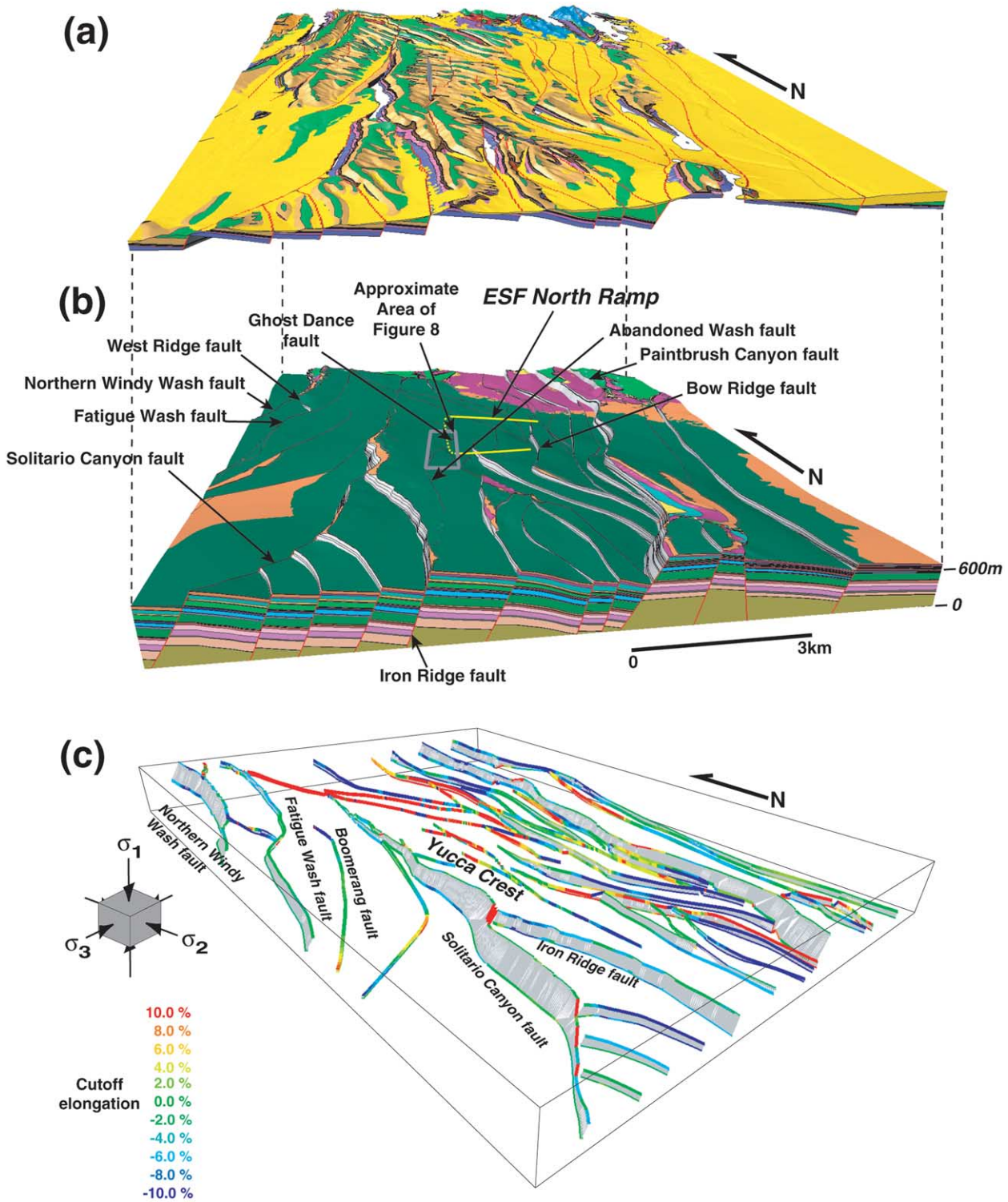

Fig. 2. Views of the Geologic Framework Model version 3.1 (CRWMS M&O, 2000b). (a) View of the model from the ground surface down to the top of the Repository Host Horizon (RHH). (b) View of the model showing the top of the RHH and underlying stratigraphy to illustrate the fault gaps. The Exploratory Studies Facility (ESF) is displayed as a solid yellow line where it lies above the RHH and a dashed yellow line where it lies within it. The Ghost Dance–Abandoned Wash fault system is highlighted by a gray rectangle. (c) View of the RHH cutoff lines against faults modeled within the Geologic Framework Model. Fault surfaces between the hanging wall and footwall cutoff lines are constructed and the model is then placed in a stress tensor field—in this case σ_1 = vertical, 21 MPa, σ_2 = horizontal, azimuth 000°, 17 MPa, and σ_3 = horizontal, azimuth 270°, 6 MPa. Here bedding is assumed to have been horizontal prior to fault motion. Cutoff elongations are calculated for each segment of each cutoff line and displayed color-coded according to the scale.

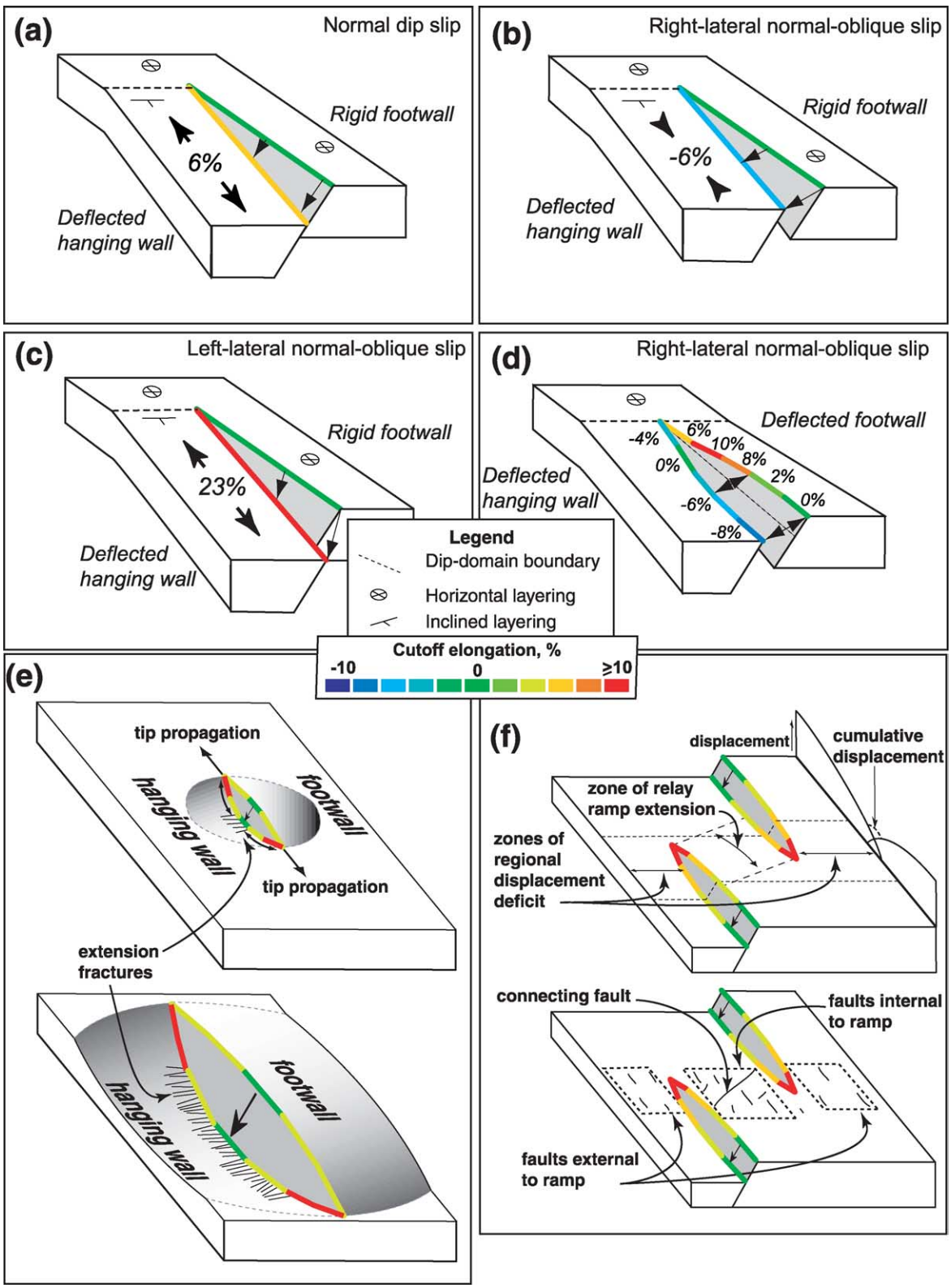

Fig. 3. Displacement gradients and distributed deformation. Cutoff lines are color-coded for elongation strain according to the color scale. (a) Rigid footwall, deformed hanging wall, dip-slip. (b) Rigid footwall, deformed hanging wall, right-lateral normal oblique-slip. (c) Rigid footwall, deformed hanging wall, left-lateral normal oblique-slip. (d) Deformed footwall and hanging wall, right-lateral normal oblique-slip, variable displacement gradient. (e) Cutoff elongation strain developed as a result of a propagating normal fault. Deformation is depicted as being preferentially partitioned into the hanging wall because this is likely common at Yucca Mountain (Ferrill and Morris, 2001). (f) Displacement deficit compensation and cutoff elongation where two faults interact, combine to develop small faults sub-parallel to, and a connecting fault oblique to the regional trend, respectively.

throws of 450 and 150 m, respectively, and are two of the largest faults that cut Yucca Mountain. Two tunnels, the Exploratory Studies Facility (ESF) and Enhanced Characterization of the Repository Block (ECRB), have been excavated in order to aid the characterization of the main repository block with respect to rock type, faults, and fractures (Mongano et al., 1999; CRWMS M&O, 2000b) (Fig. 1b). The detailed data have not been linked to the larger structural elements of Yucca Mountain, and models to assist in the prediction of small faults and fractures in areas outside the tunnels are generally lacking. In this paper, we use existing data (e.g. Day et al., 1998a,b), including that acquired by the DOE (e.g. CRWMS M&O, 1998), to evaluate displacement patterns on mapped faults at Yucca Mountain to better understand structural controls on small-scale faulting and fracturing at Yucca Mountain. Based on this analysis, we find that in areas where detailed studies have been conducted, displacements on mapped faults can be used as indicators of distributed deformation at smaller scales within the adjacent rock.

2. Background

Surface exposures at Yucca Mountain consist of faulted and fractured Miocene silicic volcanic rocks, primarily the Tiva Canyon Tuff of the Paintbrush Group (Sawyer et al., 1994). Also part of the Paintbrush Group, but less well-exposed than and stratigraphically below the Tiva Canyon Tuff, is the Topopah Spring Tuff. The DOE has designated a series of welded units within the Topopah Spring Tuff as the proposed Repository Host Horizon (RHH). Specifically, the RHH consists of the lower third of the upper lithophysal zone, and the middle nonlithophysal, lower lithophysal, and lower nonlithophysal zones of the crystal-poor member of the Topopah Spring Tuff (CRWMS M&O, 2001). The top of the RHH is represented as a horizon within the DOE Geologic Framework Model version 3.1 (CRWMS M&O, 2000b), which is a three-dimensional interpretation of the structure and stratigraphy at Yucca Mountain (Fig. 2a and b).

The structural geology of Yucca Mountain is dominated by west-dipping, extensional faults with strikes between 000° and 030° (e.g. Ferrill et al., 1999a; Figs. 1b and 2). Slip on these faults has generated the eastward-dipping fault blocks that characterize the area. Faulting developed in the Paintbrush Group tuffs at Yucca Mountain over the last 13 million years in a stress system with a vertical σ_1, initially with σ_3 directed approximately W, then evolving to the current situation with σ_3 directed toward the NW (Zoback et al., 1981; Morris et al., 1996). In addition to the dominant normal faults, small numbers of strike-slip and reverse faults have been mapped (Day et al., 1998a,b; Mongano et al., 1999).

Thus far, fault characterization at Yucca Mountain has progressed along three tracks. First, the area has been mapped by traditional field geological methods at a variety of scales (Scott and Bonk, 1984; Simonds et al., 1995; Day et al., 1998a,b). Second, fault and fracture data have been collected from detailed pavement mapping at the surface of Yucca Mountain (e.g. Barton and Hsieh, 1989; Barton et al., 1993; Barton and Larsen, 1985; Sweetkind et al., 1997; Dunne et al., 2003) with the goal of determining the influence of these structures on the infiltration of surface water into the subsurface and as analogs for fracturing that might be encountered in the subsurface. Third, the tunnel walls of the ESF and ECRB have provided detailed fault and fracture data. This dataset was collected by mapping of tunnel walls and detailed line surveys conducted during the active tunneling phase (Mongano et al., 1999; CRWMS M&O, 2000a,b; Appendix A). Traditional geological mapping is capable of detecting and representing faults with displacements greater than about 1.5 m, under favorable circumstances, or greater than 5 m elsewhere (Day et al., 1998a,b). In contrast, mapping of tunnel walls, where colluvium and vegetation do not obscure the rock, recorded faults with displacements as small as 0.02 m (Mongano et al., 1999; CRWMS M&O, 2000a).

Larger (field-mappable) faults are important indicators of the overall structure and fault block deformation at Yucca Mountain (e.g. Young et al., 1992a,b; Ferrill and Morris, 2001). Smaller faults are more difficult to detect using surface geological mapping techniques but are more numerous than larger faults. For example, the North Ramp of the ESF traverses beneath the mapped traces of 14 faults with displacements of 5–50 m (Day et al., 1998a,b), whereas mapping of the tunnel walls (CRWMS M&O, 1998, 2000a; Appendix A) of the North Ramp identified 262 faults with displacements as small as 0.02 m. Although small faults do not accommodate a major component of regional-scale deformation, they do influence permeability architecture, rockfall potential, failure strength and fracture characteristics (U.S. Department of Energy, 1998).

3. Fault displacement gradients; faults and fractures

Wherever faults exhibit displacement gradients, strain is distributed into adjacent fault blocks. Two primary components of this strain in the case of extensional faults are: (i) cutoff parallel elongation (Ferrill and Morris, 2001) (Fig. 3a–e), and (ii) strike-perpendicular distributed deformation in zones of displacement deficit, which has been recognized in the Canyonlands (Utah) (Trudgill and Cartwright, 1994), the English Midlands Coalfield (Peacock and Sanderson, 1994; Childs et al., 1995; Huggins et al., 1995), the Basin and Range of southwest USA, and the Newark Basin in the northeast USA (Anders and Schlische, 1994) (Fig. 3f). Both of these strain distribution mechanisms can be recognized at Yucca Mountain (Fig. 2b), where they are manifest as faults and fractures at scales smaller than the principal faults that generated them.

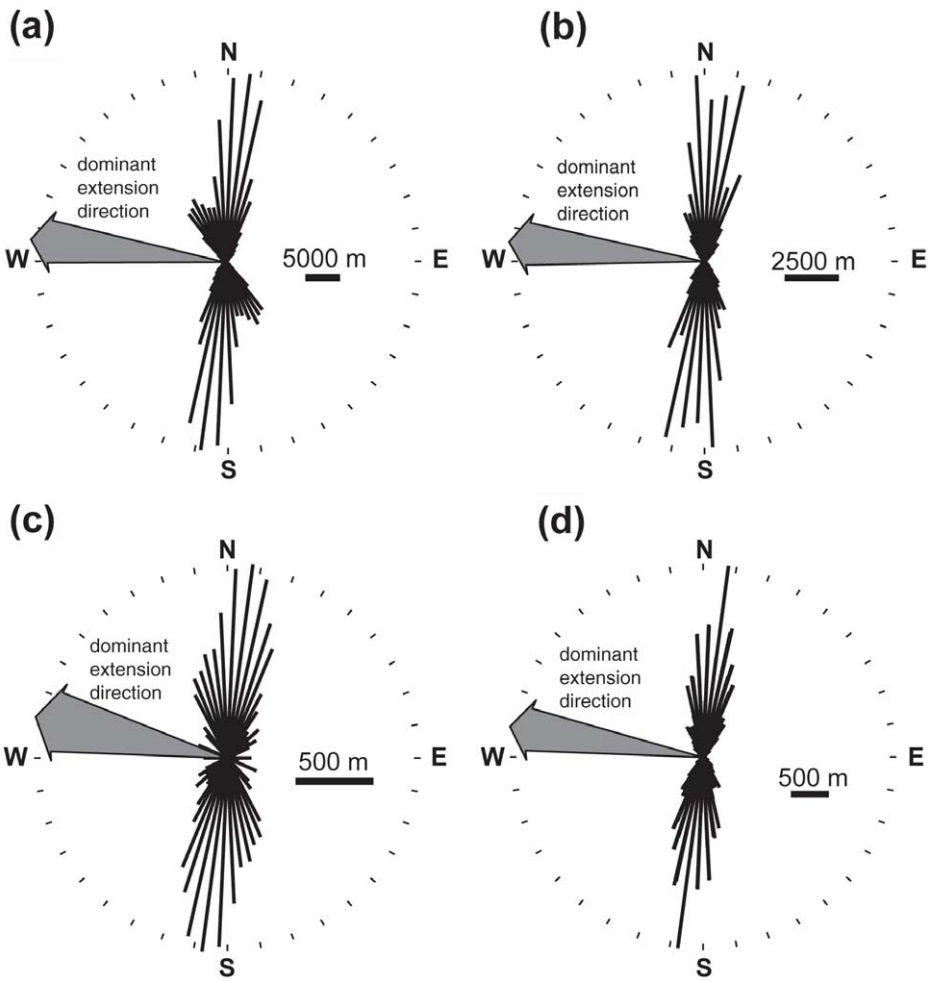

Fig. 4. Circular histograms of features indicating fault strikes at Yucca Mountain. (a) Cumulative fault trace length (data from Geologic Framework Model version 3.1 (CRWMS M&O, 2000b)), (b) Fault segment length weighted by cumulative EW heave (data from Geologic Framework Model version 3.1 (CRWMS M&O, 2000b)), (c) Scarps and lineaments in alluvium indicating probable late Quaternary fault motion (data from Simonds et al., 1995), (d) Fault traces, bedrock–alluvium contacts and other features indicating possible late Quaternary fault motion (data from Simonds et al., 1995).

3.1. Cutoff-parallel elongation

Fault-cutoff-parallel elongations experienced by rock adjacent to faults are determined by fault displacement gradients, fault slip vectors, and initial stratal orientations (Ferrill and Morris, 2001). Elongation parallel to the stratal cutoff line (line of intersection between rock strata and fault plane) can be positive (length increase; Fig. 3a, c and d) or negative (length decrease; Fig. 3b and d) and depends only on angular relationships (Ferrill and Morris, 2001). Therefore, the elongation can be calculated for sections of a fault between cutoff line data points. Details of stratal cutoff lines for all principal geologic strata (horizons) at Yucca Mountain can be extracted from the DOE Geologic Framework Model (CRWMS M&O, 2000b; Fig. 2a and b). The resulting data can be assembled into a 3D fault gap model for any given horizon. In this paper we use a fault gap model for the top of the RHH generated from data within the DOE Geologic Framework Model (CRWMS M&O, 2000b) (Fig. 2b), because it is the top of the lithologic package that the DOE has selected to host the proposed repository.

3.1.1. Fault slip vectors

Using the 3D fault gap model, detailed geometry of the fault surfaces between offset cutoff lines can be generated (Fig. 2c). These surfaces can then be used to determine the slip vector field throughout the study area. This is done by using slip tendency analysis (Morris et al., 1996) to investigate a range of stress systems likely to have been extant at the time of faulting. In computing slip tendency, the directions of maximum resolved shear stress on a fault surface are computed. For any portion of the fault surface, the direction of maximum resolved shear stress is the probable slip direction (e.g. Bott, 1959; Morris et al., 1996). Each stress system will yield a unique slip vector field. By using a range of stress systems likely to have been operating during faulting, a range of slip vector fields can be computed, and their effects on cutoff elongation can be examined.

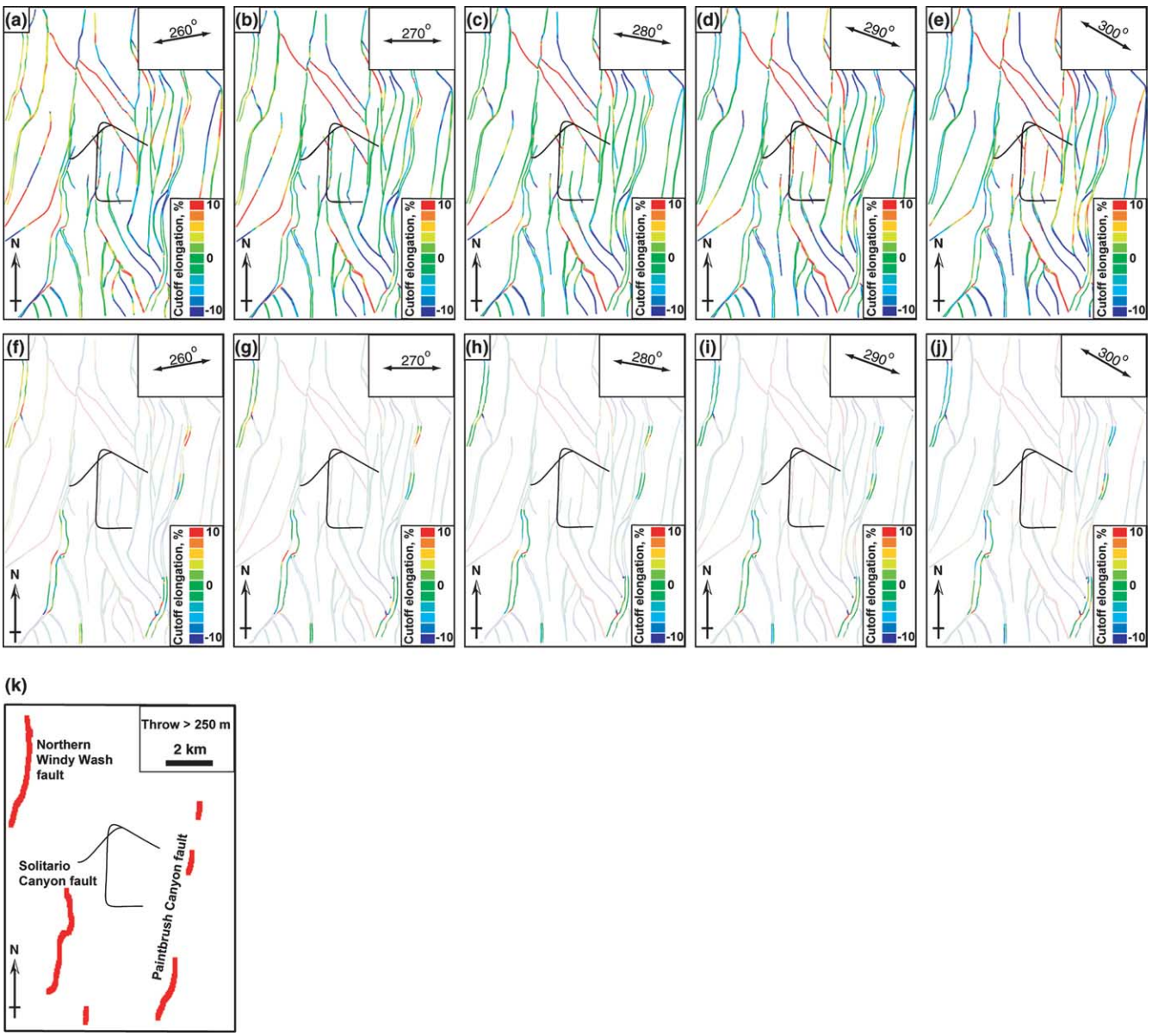

Fig. 5. (a)–(e). Series of five cutoff elongation maps illustrating a simple tectonic history for Yucca Mountain in which regional extension rotates progressively clockwise from 260 to 300°. Maps of traces of faults at Yucca Mountain where they intersect with the Repository Host Horizon (data extracted from the DOE Geologic Framework Model version 3.1 (CRWMS M&O, 2000b)). The cutoff elongation for each segment of the cutoff lines is displayed color-coded according to the scale in 2% increments. All cutoff lines in each map are modeled as subject to the same stress tensor throughout the map and assuming a horizontal (pre-faulting) bedding orientation. (f)–(j) Maps (a)–(e) showing only fault traces that have experienced greater than 250 m of throw. (k) Map of the distribution of fault segments with throw values greater than 250 m.

The period of most active faulting at Yucca Mountain is generally thought to have been during the Miocene (13–10 Ma) (Sawyer et al., 1994; Morris et al., 1996; Snow and Wernicke, 2000). At that time, the orientation of extension (i.e. minimum principal stress) was between WSW (260°) and NW (300°) (Zoback et al., 1981; Morris et al., 1996). Vertical principal stress for input into the analysis was determined primarily by assuming lithostatic loading, which is approximately 21 MPa at a depth of about 1 km for rocks with densities similar to those at Yucca Mountain (Ferrill et al., 1999b). In order for the rocks to have been close to failure, and thus to have experienced active faulting, the differential stress ($\sigma_1 - \sigma_3$) at 1 km depth must have been approximately 15 MPa (Hoek and Brown, 1988; Mandl, 1988), therefore the minimum stress (σ_3) would have been on the order of 6 MPa. Given these two constraints, σ_2 could have varied within these limits. High values of σ_2 (low values of the stress ratio R, where $R = (\sigma_1 - \sigma_2)/(\sigma_1 - \sigma_3)$) give rise to conditions conducive to both normal and strike-slip faulting (Morris et al., 1996). Lower σ_2 (and higher R) values would give rise to less strike-slip faulting.

Data from borehole breakouts, active faulting, earthquake nodal planes, and fault orientations indicate that Yucca Mountain currently experiences a normal faulting

regional stress condition with σ_3 oriented approximately NW (300° azimuth), and a σ_2 value close to that of σ_1 (Stock et al., 1985; Stock and Healy, 1988; Harmsen, 1994; Morris et al., 1996; Ferrill et al., 1999b). This stress system accounts for the dominance of normal faulting in the area and the synchronous oblique-slip to strike-slip activity on many NW-striking faults. It is also consistent with interpretations of the slip events associated with the 1992 Little Skull Mountain earthquake (Harmsen, 1994; Morris et al., 1996) which occurred at a depth of about 8 km, 16 km ESE of Yucca Mountain.

Models of the Cenozoic tectonic evolution of North America, during which the Juan de Fuca Ridge was subducted beneath North America creating the San Andreas fault system (Atwater, 1970; Snow and Wernicke, 2000) explain the transition of the Great Basin from compressional to extensional tectonics. Within this context, extension at Yucca Mountain has reached its current orientation by clockwise rotation of the stress field around a vertical axis since about 20 Ma (Zoback et al., 1981; Morris et al., 1996). Zoback et al. (1981) show an orientation of approximately WSW for horizontal extension during the time period 20–10 Ma and an extension direction of WNW from 10 Ma to the present (Zoback et al., 1981). Strikes of normal faults that cut the 12.8 Ma and younger volcanic rocks at Yucca Mountain show a pronounced maximum from 005° to 015°, as seen in a length-weighted circular histogram (Fig. 4a). A heave-weighted circular histogram of normal fault strike directions (Fig. 4b) exhibits a similar, but broader maximum (from 355° to 015°). Variability in the orientations of normal faults could indicate rotation of extension direction with time; however, the great preponderance of data indicating an approximately west-directed extension direction (azimuth of 265° to 285°; Fig. 4a–d) suggests that most deformation occurred, or at least initiated, early in the rotation history. In the context of the analysis presented in this paper, stress rotation during the last 12.8 million years modifies the detailed character and distribution of cutoff elongation (Fig. 5a–e).

3.1.2. Initial stratal orientation

The orientation of a stratal cutoff line with respect to the slip vector influences the nature and magnitude of the elongation experienced by that cutoff line (Ferrill and Morris, 2001). In the case of the volcanic tuffs at Yucca Mountain, strata were probably sub-horizontal prior to faulting. However, as faulting progressed, an east dip developed in fault blocks. The increasing east dip of strata modified the detailed character and distribution of cutoff elongation.

3.2. Progressive deformation at Yucca Mountain

Deformation in fault blocks starts with the initiation of fault displacement and continues to accumulate over time with each increment of fault slip. This progressive deformation of fault blocks is in accord with changing stress state, fault geometry, and stratal orientation. The deformation state at any given time is the result of this accumulated deformation. Single maps of fault cutoff elongation cannot capture the full deformation history. For example, early in the history of faulting, when the regional extension direction was approximately WSW, there would have been fewer, shorter, and smaller (in terms of displacement) faults at Yucca Mountain than are currently present, similar to the early stages of extensional fault system development seen in analog model experiments (Ackermann et al., 2001; Sims et al., 2004). Extension direction has rotated over time, and as faults grew, the slip vectors on those faults would have changed concomitantly with the changing stress conditions and fault orientations. Fault growth would also have controlled stratal dip in fault blocks and, consequently, cutoff line orientations would have evolved through time.

Fault cutoff maps have been constructed for all the present-day faults represented in the DOE Geologic Framework Model, version 3.1 (CRWMS M&O, 2000b) using a range of stress tensor magnitudes and orientations and initial stratal dips. For each case, all faults are subjected to the same regional stress system and conditions of initial stratal orientation. Faults with orientations that deviate markedly from the regional average probably initiated in response to local variations in the regional stress system (the result of displacement gradients on the larger faults), and therefore the modeled cutoff elongations would only apply when the local perturbation had been relieved by slip on that fault or faults. Once the local perturbation had been relieved, the fault responded to the full regional stress field, and either the modeled elongations became relevant, or the fault became inactive as its slip tendency fell below the threshold for slip. These maps are illustrated in Appendix B and represent the likely range of conditions that could have been experienced at Yucca Mountain. As such, they are a means for assessing the likelihood that fault blocks have experienced significant strain resulting from fault cutoff elongation in a variety of local tectonic scenarios.

3.2.1. Cutoff elongation maps

The earliest extension direction experienced by the volcanic rocks at Yucca Mountain was probably 260° (Zoback et al., 1981; Fig. 5). At that time (12.8 Ma), the newly erupted rocks were probably close to horizontal in orientation. The strong preferred orientation of all faults (Fig. 4) and the common occurrence of near strike-slip motion on NW–SE-trending faults indicates a stress magnitude ratio R that is low, approximately 0.25–0.3 (Morris et al., 1996). Since about 10 Ma the extension direction at Yucca Mountain has rotated clockwise to about 300°. Therefore a simple tectonic history would be characterized by a stress tensor of $\sigma_1 = 21$ MPa (vertical), $\sigma_2 = 17$ MPa, and $\sigma_3 = 6$ MPa (horizontal), and that

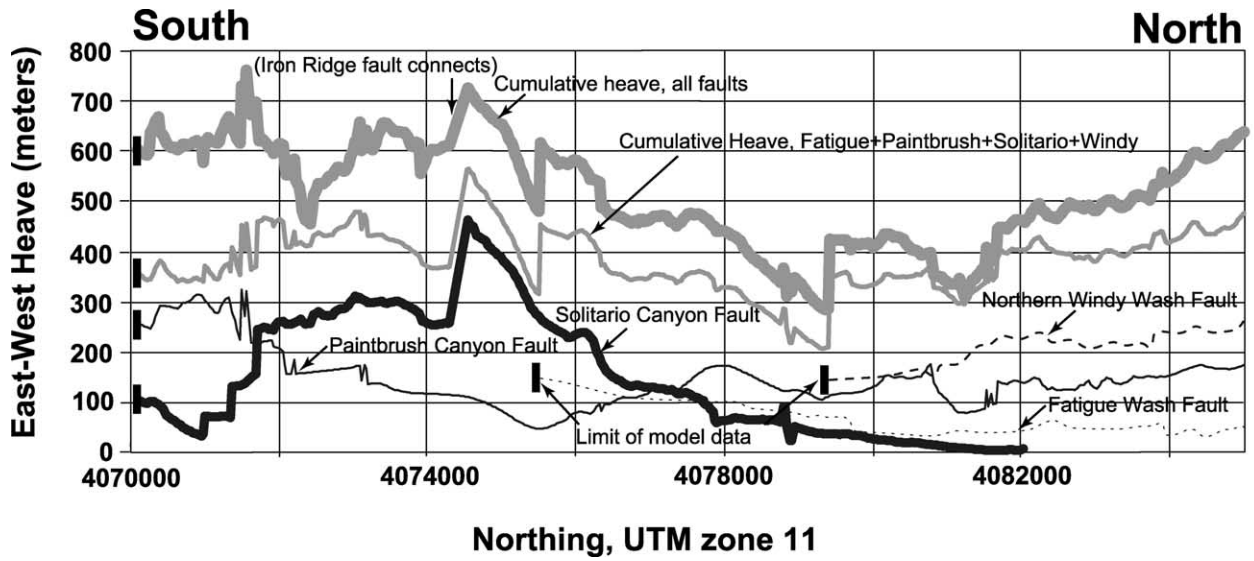

Fig. 6. East–west component of horizontal displacement (heave) on the major faults at Yucca Mountain. Plotted here are the heave profiles for the Solitario Canyon (thick black line), Paintbrush Canyon (thin black line), Northern Windy Wash (dashed black line), and Fatigue Wash faults (dotted black line). In addition, the cumulative (combined) heave of these four faults (thin gray line) is shown together with the cumulative heave of all faults (thick gray line) within the DOE Geologic Framework Model version 3.1. Bold vertical lines at the ends of lines indicate the points at which the faults are truncated by the edges of the model.

rotated 40° clockwise about a vertical axis from 12.8 Ma to present. Simplicity would also dictate initially horizontal beds throughout. Therefore, using this simple interpretation of the local tectonic history, cutoff elongation strains at Yucca Mountain over the last 12.8 Ma can be portrayed by Fig. 5a–e. The principal source of uncertainty in these maps is the number of faults represented; it is likely that many of the faults shown would not have existed throughout the time of active faulting. Those that did exist were likely shorter and accommodated less displacement than they now exhibit.

3.2.2. Interpretation of cutoff elongation maps

Cutoff elongation strains calculated using the method described by Ferrill and Morris (2001) are scale independent: they take no account of the magnitude of the volume of rock affected. However, a large-displacement fault with high cutoff elongation will affect a large volume of adjacent fault block compared with a small-displacement fault that has similarly high cutoff strains. Thus, small-displacement faults may not generate map scale strain features as a result of cutoff elongation strains. The greatest effects of fault cutoff elongation are likely to be manifest where fault displacement is greatest. Fig. 5k illustrates the geographic distribution of fault sections that have throws greater than 250 m. Using these large-throw fault sections as a screen to suppress faults with smaller throw for maps in Fig. 5a–e yields the maps in Fig. 5f–j. Portions of these large-throw fault sections also have high values of cutoff elongation and are thus more likely to have generated mappable deformation features. There are five principal areas that exhibit both high throw and high strain consistently over the last 12.8 million years.

The Northern Windy Wash fault and its interaction with the Fatigue Wash fault through the West Ridge connecting fault system (Figs. 1b and 2) has already been identified as an area of high cutoff elongation strain, and is discussed in detail by Ferrill and Morris (2001). An approximately 5-km-long portion of the Solitario Canyon fault (Figs. 1b and 2) also exhibits both high throw and high cutoff elongation strain (Fig. 5). This section of the Solitario Canyon fault connects with four other faults at angles of 60–80°. Three sections of the Paintbrush Canyon fault have both high throw and high cutoff elongation strain (Fig. 5). Of these, the northern two are inferred fault traces covered by alluvium and are not considered further. The southernmost section is exposed in part, and two fault branch lines coincide with zones of high cutoff elongation strain (Figs. 1b, 2 and 5). Fault branching at high angles to the principal fault are manifestations of cutoff elongation strain accommodated by map scale faults. Other faults that exhibit high values of cutoff elongation strain are likely to have generated structures that accommodate this strain but because total displacement is small, the scale of these structures is commensurately small and they have not been recorded by field mapping.

3.3. Segmented faults and distributed deformation

Displacement patterns on the four dominant faults at Yucca Mountain (Northern Windy Wash, Fatigue Wash, Solitario Canyon, and Paintbrush Canyon faults; Figs. 5k

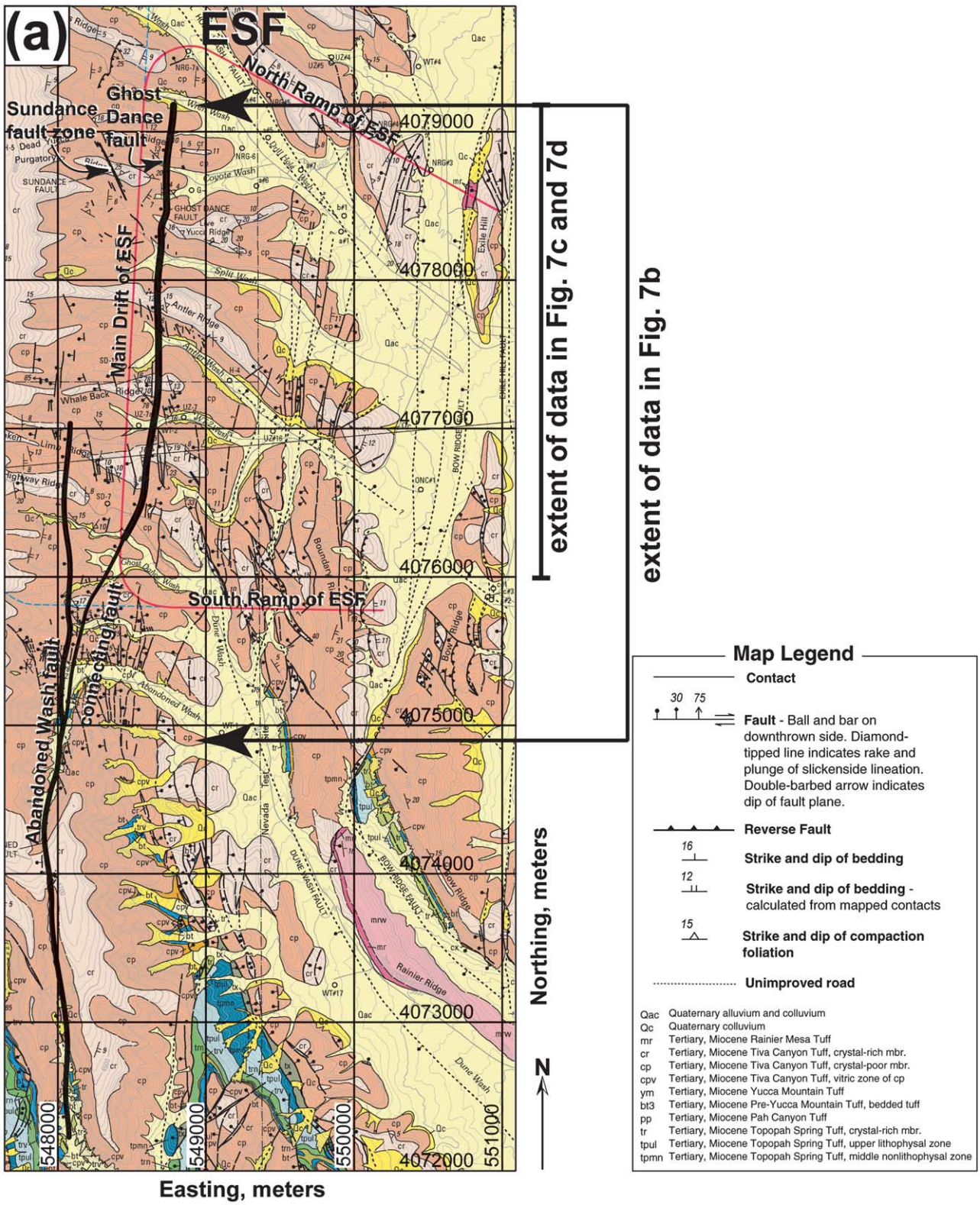

Fig. 7. The Ghost Dance–Abandoned Wash fault system. (a) Map from Day et al. (1998a) with the Ghost Dance and Abandoned Wash faults highlighted, together with the connecting fault that breaches the extensional relay ramp between the two faults. The northing scales of (b)–(d) are the same. (b) Throw profiles of the Ghost Dance–Abandoned Wash fault system for the interval: northing = 4074850–4079150 m, using data from the DOE Geologic Framework Model version 3.1 (CRWMS M&O, 2000b). (c) Throw gradient along the Ghost Dance fault (thick black line) and part of the connecting fault (thin black line) plotted against fracture intensity (number of fractures per 5 m interval: black dots; 12 cycle moving average of 5 m interval data: thick gray line) for 16,570 fractures in the Exploratory Studies Facility (ESF) Main Drift tunnel for interval: northing = 4076000–4079150 m (Appendix A). See text for discussion. (d) Strike of 16,570 fractures within the ESF Main Drift tunnel (Appendix A) for the same interval of northing as (c). Note the continuous change in strike of the strongest orientation cluster from north (strike approximately 110°) to south (strike approximately 150°).

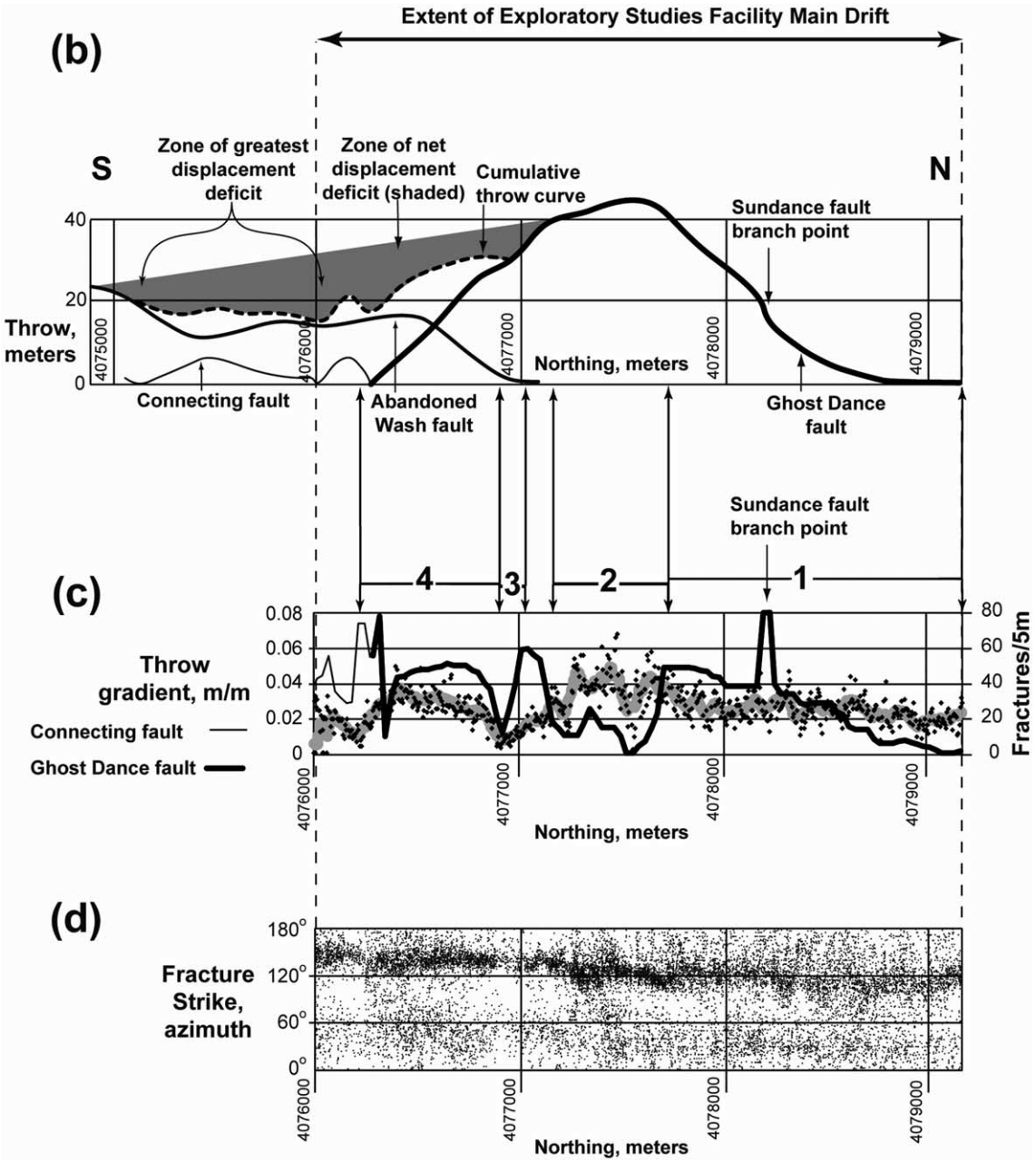

Fig. 7 (*continued*)

and 6) indicate that they have operated as part of a segmented fault system in which the collective assemblage of faults has a coherent cumulative displacement profile (e.g. Walsh and Watterson, 1991; Anders and Schlische, 1994; Peacock and Sanderson, 1994; Dawers and Anders, 1995; Huggins et al., 1995; Willemse et al., 1996; Ferrill et al., 1999a; Walsh et al., 2003), and therefore have the potential to rupture in concert in the event of a major earthquake (Anders and Schlische, 1994; Ferrill et al., 1999a). The Paintbrush Canyon and Solitario Canyon faults, for example, have an inverse displacement relationship south of about 4077000 (UTM northing in meters) (Fig. 6); north of 4077000 the inverse relationship continues, although the combined heave of these faults decreases. This local decrease (deficit) in cumulative heave is in part compensated for by the presence of both the Northern Windy Wash and Fatigue Wash faults. At approximately 4074500 there is a drop in the heave of both the Solitario Canyon and Paintbrush Canyon faults, this is where the Iron Ridge fault (not plotted in Fig. 6) connects with the Solitario Canyon fault and accommodates a significant proportion of the total heave. Other apparent heave deficits in the cumulative heave profile (at approximately 4075500 and 4079200) are not real, but are the result of data truncation on the Northern Windy Wash and Fatigue

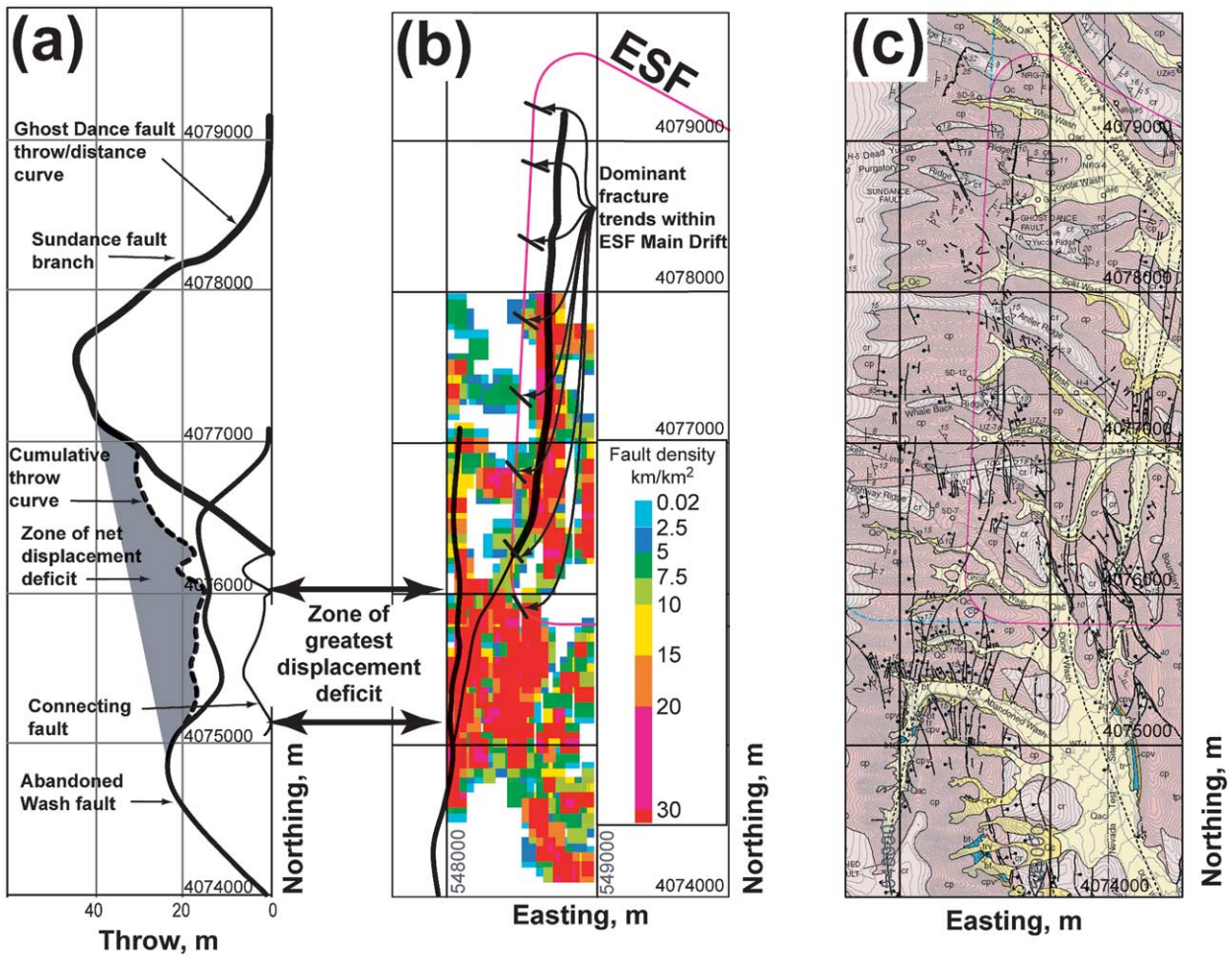

Fig. 8. (a) Throw profiles of the Ghost Dance–Abandoned Wash fault system for the interval: northing = 4074000–4079150 m, using data from the DOE Geologic Framework Model version 3.1 (CRWMS M&O, 2000b). (b) Outline map of the Ghost Dance–Abandoned Wash fault system with the predominant fault and fracture orientations for each 500 m section (arrowed) of the Exploratory Studies Facility Main Drift (Mongano et al., 1999). Superimposed on the area of interaction between the Ghost Dance and Abandoned Wash faults is a map of fault density calculated as fault trace length per area (km/km^2) for a 100 m by 100 m window moved in increments of 50 m both EW and NS. Note that the color scale of fault density is not linear. Fault traces were extracted from the Day et al. (1998a) map as shown in (c).

Wash faults at the western edge of the DOE Geologic Framework Model version 3.1 volume (CRWMS M&O, 2000b). Transfer of displacement between two overlapping extensional faults can be accomplished in a number of ways, for example increased stratal dip in the area of interaction is commonly observed (Huggins et al., 1995), as is an increase in the number of smaller faults and fractures contributing to the regional extension in the area of overlap between principal faults (e.g. Anders and Schlische, 1994). However, this fault and fracture density increase is not necessarily confined to overlap zones or relay ramps (Fig. 3f). Such an increase is an important component of fault block deformation in the Ghost Dance–Abandoned Wash fault system at Yucca Mountain.

4. Ghost Dance–Abandoned Wash fault system

Using a combination of geologic maps and data from the Department of Energy's Geologic Framework Model version 3.1 (CRWMS M&O, 2000b), we have identified an area of interaction between the Ghost Dance and Abandoned Wash faults (Area 4 in figure 9a of Ferrill and Morris, 2001). This area is of special interest because the Ghost Dance fault intersects the ESF (Fig. 7a). This area represents one of the few opportunities to evaluate extremely detailed fault and fracture data in the context of the larger faults mapped by traditional field geological methods. Fault and fracture mapping of the ESF Main Drift (azimuth 183°) documents 16,570 fractures in this section of tunnel (CRWMS M&O, 1998, 2000a,b; Appendix A).

4.1. Analysis of Ghost Dance fault displacements and ESF fracture data

4.1.1. Description

Graphs of throw and cumulative throw versus northing were prepared for the Ghost Dance, Abandoned Wash, and

Connecting faults from 4074850 to 4079100 m northing (Fig. 7b). Throw gradient was calculated for the Ghost Dance and Connecting faults (thick and thin black lines, respectively, in Fig. 7c) over the northing interval where these faults run parallel and adjacent to the Main Drift of the ESF. Plotted against the throw gradient curve is a measure of fracture intensity (number of fractures per 5 m interval of tunnel) derived from the fractures mapped in the Main Drift tunnel (CRWMS M&O, 1998, 2000a,b; Appendix A; thick gray line in Fig. 7c) which lies entirely within the Topopah Spring, welded, lithophysal-poor tuff (Tsw2) (CRWMS M&O, 1998). To represent the variation in fracture trend, the strikes of all 16,570 fractures are plotted against northing (Fig. 7d). We have defined four areas that illustrate the relationship between fault displacement patterns and fracture intensity; these are labeled 1–4 in Fig. 7b and c.

4.1.1.1. Area 1: northing interval 4079100–4077700 m. Both throw gradient on the Ghost Dance fault and fracture intensity in the Main Drift tunnel increase more or less continuously from north to south. The throw gradient curve has a major spike where the Sundance fault joins the Ghost Dance fault obliquely, which is not reflected in the fracture intensity data (Fig. 7a–c). The Sundance fault is a NW-trending fault, mapped in the hanging wall of the Ghost Dance fault north of about 4077700 m northing. Although in Fig. 7a (after Day et al., 1998a) the Sundance fault is shown as discontinuous, other workers show this fault connecting with the Ghost Dance fault at about 4077700 m northing (CRWMS M&O, 2000b).

4.1.1.2. Area 2: northing interval 4077700–4077150 m. The throw gradient on the Ghost Dance fault exhibits a broad minimum roughly coincident with the throw maximum on the Ghost Dance fault (Fig. 7a and b). Within this broad throw gradient low is a double maxima high. Over the same interval the fracture intensity data define a complex broad peak.

4.1.1.3. Area 3: northing interval 4077050–4076925 m. The throw gradient has a sharp peak and trough near the tip of the Abandoned Wash fault and the northern part of the overlap zone between the Ghost Dance and Abandoned Wash faults. Fracture intensity falls to a minimum, coincident with the throw gradient minimum.

4.1.1.4. Area 4: northing interval 4076925–4076250 m. A broad high in throw gradient marks most of the remainder of the overlap zone between the Ghost Dance and Abandoned Wash faults, with a sharp spike at the tip of the Ghost Dance fault. The fracture intensity data also exhibits a high that is approximately coincident with the throw gradient high.

4.1.1.5. Fracture orientations. The predominant strike of fractures in the ESF changes smoothly and continuously from 110° to 150° from north to south along the Main Drift over a distance of about 2.5 km (Fig. 7d). A less well-defined, orthogonal population of fractures exhibits a similar variation. Between northing 4079100 and 4078500 m the strike of the most prominent fractures observed within the Main Drift of the ESF is approximately 75–80° from the strike of the Ghost Dance fault (Fig. 8b). South of 4078500 m N, the angle between the most prominent fracture trend and the Ghost Dance fault decreases to 65–70°, and this angular difference is maintained as the Ghost Dance fault changes strike within its zone of interaction with the Abandoned Wash fault.

4.1.2. Interpretation

We interpret the close correspondence between the pattern of throw gradient on the Ghost Dance fault and fracture intensity observed in the ESF primarily as the result of cutoff-parallel elongation. There are three cases, one in each of Areas 1–3, where there is a mismatch between the throw gradient and fracture intensity curves.

4.1.2.1. Area 1: northing interval 4079100–4077700 m. Where the Sundance fault intersects the Ghost Dance fault (Fig. 7a–c) there is a spike in the throw gradient (Fig. 7c), which is not reflected by a similar spike in the fracture intensity data. The throw gradient intersection point with the Sundance fault and the location of the Sundance fault in the ESF tunnel do not share the same northing value because the Sundance fault is oblique to the Ghost Dance fault and ESF. The lack of increased fracturing is likely the result of the Sundance fault having accommodated the throw gradient, obviating the need for increased fracture intensity.

4.1.2.2. Area 2: northing interval 4077700–4077150 m. The broad low in the Ghost Dance fault throw gradient (thick line in Fig. 7c) is matched by a broad high in the fracture intensity curve (thick gray line in Fig. 7c). This is also the region of greatest throw on the Ghost Dance fault (Fig. 7b). Within the throw gradient low is a double maxima high which closely corresponds to the shape of the fracture intensity peak. Although this portion of the Ghost Dance fault does not currently exhibit high throw gradients, it is the location on the fault of greatest total slip, and therefore the potential for having accumulated damage in rocks adjacent to the fault is greater here than anywhere else along the fault.

4.1.2.3. Area 3: northing interval 4077050–4076925 m. The third area of mismatch, at about northing 4077050 m (Fig. 7c), is enigmatic and we currently have no good explanation for its presence.

4.1.2.4. Fracture orientations. The principal fractures present in the Main Drift of the ESF are likely the result of the cutoff-parallel elongation generated by slip on the Ghost Dance fault. North of the zone of interaction with the Abandoned Wash fault these fractures formed at a high

angle to the fault strike. This angle decreases into the zone of overlap and net displacement deficit because the bulk extension direction in this zone is rotated clockwise to accommodate the fault-strike-perpendicular component of extension resulting from the displacement deficit (e.g. Anders and Schlische, 1994; and see below). Using an independent approach, based on stress perturbations resulting from fault displacement gradients during active faulting, Dunne et al. (2003) found that extension fractures would form at high angles to fault strike in cooling tuffs erupted immediately prior to fault slip (Sweetkind et al., 2004).

4.2. Analysis of fault-perpendicular extension in the Ghost Dance–Abandoned Wash fault system

4.2.1. Description

An extensional fault relay ramp (e g. Childs et al., 1995) has developed between the Ghost Dance and Abandoned Wash faults (Ferrill and Morris, 2001). A connecting fault has been mapped (Day et al., 1998a,b) that breaches the ramp and connects the Ghost Dance and Abandoned Wash faults (Fig. 7). We define the zone of interaction between the Ghost Dance and Abandoned Wash faults as the area of overlap between the two main faults, plus the extent of the connecting fault (between 4075000 and 4077000 m north; Fig. 7). Summing throw on the Ghost Dance, Abandoned Wash, and Connecting faults reveals a local decrease in the cumulative displacement between 4075000 and 4077000 m north, and a zone of greatest displacement deficit between about 4075200 and 4076000 m north (Figs. 7b and 8a). The zone of greatest displacement deficit is not within the overlap between the Ghost Dance and Abandoned Wash faults (Fig. 8a and b). Using the map of Day et al. (1998a) we measured fault densities in an area encompassing the zone of interaction between the Ghost Dance and Abandoned Wash faults (Fig. 8). Fault density is here defined as total fault trace length per unit area. We used a 100-m-square moving window (increment of movement = 50 m) to calculate densities (as km/km^2), and these are plotted in Fig. 8b.

4.2.2. Interpretation

The area of highest fault density has a north–south extent that is coincident with the zone of greatest displacement deficit on the principal, adjacent faults (Ghost Dance, Abandoned Wash and connecting faults; Fig. 8a and b). Furthermore, these faults have similar orientations to the principal faults. We interpret this high density of smaller scale, intrablock, faulting as displacement compensation for the displacement deficit on the principal faults (Fig. 8a and b). Such displacement partitioning need not be confined to the area of overlap between faults.

5. Conclusions

Detailed analyses of the data available for Yucca Mountain reveal that displacement distributions on the larger faults have a strong influence on the orientation and distribution of smaller faults and fractures. Two aspects of displacement-driven deformation are cutoff elongation and displacement deficit compensation.

Cutoff elongation and the resulting distribution and orientation of fractures within fault blocks are sensitive to: stress system, resulting slip directions at the time of faulting, and the initial bed orientation. Analyses of strains generated by fault displacement gradients indicate that some parts of Yucca Mountain have experienced sufficient cutoff elongation coupled with high fault displacement to generate map scale structures to accommodate the strain. At a smaller scale, fracture intensities recorded by detailed mapping within the ESF tunnel can be interpreted within the context of displacement patterns on the adjacent Ghost Dance fault. The variable extension direction at Yucca Mountain since the inception of faulting (about 12.8 Ma) suggests that cumulative strain patterns are likely complex and strains generated by fault displacement are more pervasive than a single stress state ‘snapshot’ would suggest.

Displacement deficit compensation is illustrated by the example of the Ghost Dance–Abandoned Wash fault system. The area of interaction between these two faults exhibits a marked cumulative displacement deficit, not confined to the area of overlap between the principal faults. This area contains a large number of small faults oriented sub-parallel to the larger faults and contributing to the overall extension. The fault density in this locality is anomalously high, approximately twice that of surrounding areas outside the influence of the displacement deficit zone.

We have shown that there is considerable variability in terms of orientation and intensity in the fault and fracture framework of Yucca Mountain. It should be recognized that different fault blocks experience different deformation histories, producing different strain states. Analysis of the fault and fracture framework of any fault block would benefit from considering the possibility that displacement patterns on bounding faults have influenced strain intensity and hence caused variability in the orientation and intensity of small-scale faulting and fracturing.

Acknowledgements

This paper was prepared to document work performed by the Center for Nuclear Waste Regulatory Analyses (CNWRA) for the U.S. Nuclear Regulatory Commission (NRC) under contract No. NRC-02-97-009. The activities reported here were performed on behalf of the NRC Office of Nuclear Material Safety and Safeguards, Division of Waste Management. This paper is an independent product of the CNWRA and does not necessarily reflect the views or

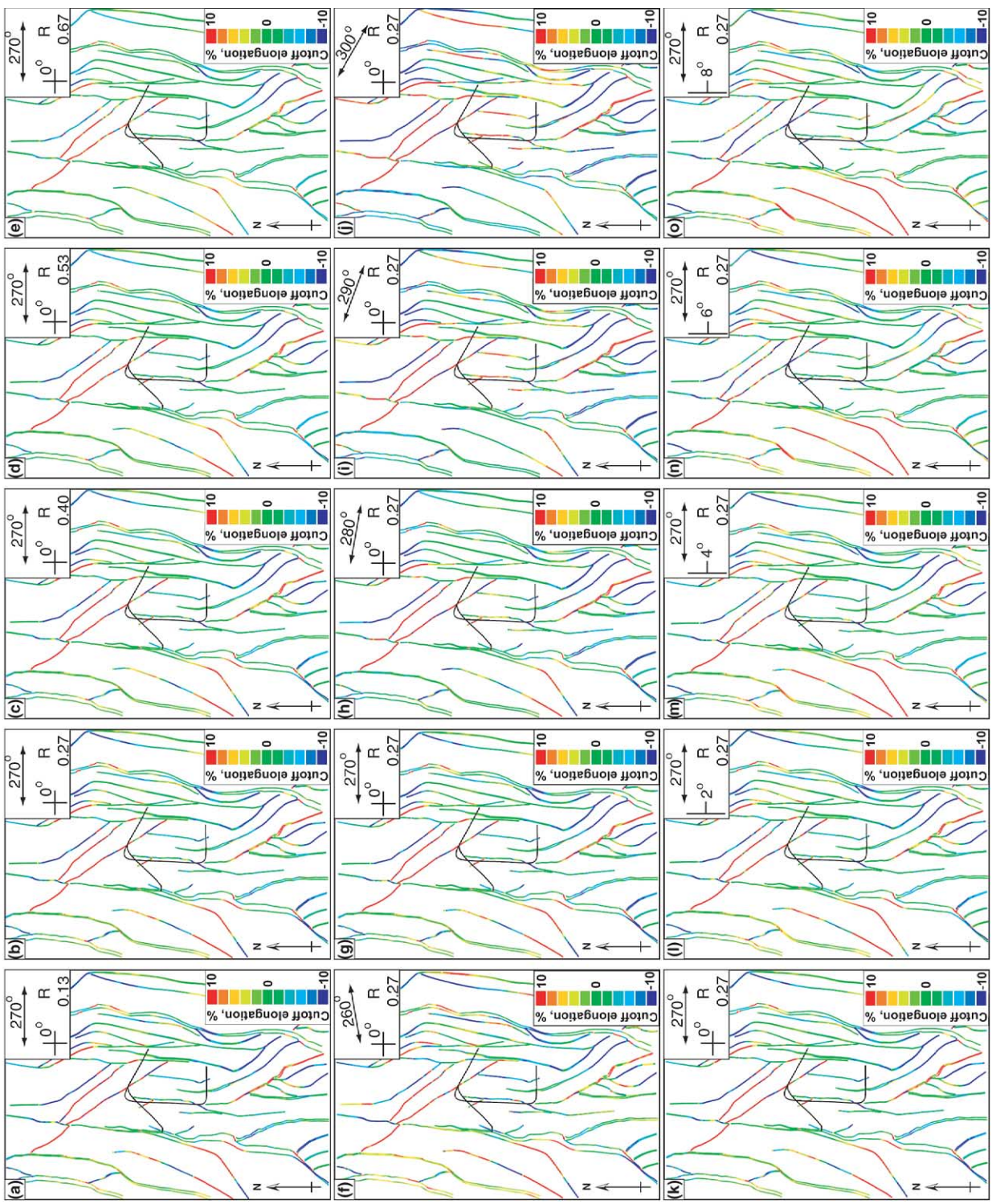

Fig. A1. Cutoff elongation maps.

Table A1
Magnitudes of maximum (σ_1), intermediate (σ_2), and minimum (σ_3) principal compressive stresses, R values, extension directions, and original bed dips used for cutoff elongation analyses are shown in maps a–o in Appendix B

Map in Appendix B	σ_1 (MPa)	σ_2 (MPa)	σ_3 (MPa)	R	Extension direction	Original bed dip
a	21	19	6	0.13	270	0
b	21	17	6	0.27	270	0
c	21	15	6	0.40	270	0
d	21	13	6	0.53	270	0
e	21	11	6	0.67	270	0
f	21	17	6	0.27	260	0
g	21	17	6	0.27	270	0
h	21	17	6	0.27	280	0
i	21	17	6	0.27	290	0
j	21	17	6	0.27	300	0
k	21	17	6	0.27	270	0
l	21	17	6	0.27	270	2
m	21	17	6	0.27	270	4
n	21	17	6	0.27	270	6
o	21	17	6	0.27	270	8

regulatory position of the NRC. We thank Philip Justus for many discussions regarding faults and fractures at Yucca Mountain. Reviews by H. Lawrence McKague, John Stamatakos, Wesley Patrick, Mark Anders, and Conrad Childs significantly improved earlier versions of this manuscript. We also thank Rebecca Emmot for assistance with manuscript preparation.

Appendix A

Fault and fracture data from the ESF were used in this paper. These data are described and referenced in CRWMS M&O (2000a) as: Data Tracking Number (DTN): MO9904MWDFPG16.000; File: zz_sep_215405.txt; File description: S99189_001 DATA REPORT. Table description: Fracture attitude data for full periphery geotechnical mapping of strike and dip data entry correction analysis, 10/07/1998 to 03/19/1999. TDIF: 308156 (Table A1).

Appendix B

A series of 15 cutoff elongation maps (Fig. A1) illustrating the influence of stress tensor R value (see equation in Section 3.1.1; maps a–e), direction of extension (σ_3; maps f–j), and stratal orientation (dip; maps k–o) at the time of fault initiation. Controlling parameters are listed in Table A1. The maps are traces of faults at Yucca Mountain where they intersect with the RHH (data extracted from the DOE Geologic Framework Model version 3.1 (CRWMS M&O, 2000b)). The cutoff elongation for each segment of the cutoff lines is color-coded according to the scale in 2% increments. All cutoff lines in each map are modeled as subject to the same stress tensor throughout the map and assuming the same initial (pre-faulting) bedding orientation. Each map illustrates different conditions of stress and initial bedding orientation and these conditions are shown in the inset at top right of each map.

References

Ackermann, R.V., Schlische, R.W., Withjack, M.O., 2001. The geometric and statistical evolution of normal fault systems: an experimental study of the effects of mechanical layer thickness on scaling laws. Journal of Structural Geology 23, 1803–1819.

Anders, M.H., Schlische, R.W., 1994. Overlapping faults, intrabasin highs, and the growth of normal faults. Journal of Geology 102, 165–180.

Atwater, T., 1970. Implications of plate tectonics for the Cenozoic tectonic evolution of western North America. Geological Society of America Bulletin 81, 3513–3536.

Barton, C.C., Hsieh, P.A., 1989. Physical and Hydrologic-flow Properties of Fractures, American Geophysical Union, Washington, DC.

Barton, C.C., Larsen, E., 1985. Fractal geometry of two-dimension fracture networks at Yucca Mountain. In: Stephanson, O. (Ed.), Fundamentals of Rock Joints. Proceedings of the International Symposium on Fundamentals of Rock Joints. Sweden, Bjorkliden, pp. 77–84.

Barton, C.C., Larsen, E., Page, W.R., Howard, T.M., 1993. Characterizing fractured rock for fluid-flow, geomechanical, and paleostress modeling: methods and preliminary results from Yucca Mountain, Nevada. U.S. Geological Survey Open-File Report 93-269.

Bott, M.H.P., 1959. The mechanics of oblique slip faulting. Geological Magazine 96, 109–117.

Buesch, D.C., Spengler, R.W., 1998. Character of the middle nonlithophysal zone of the Topopah Spring Tuff at Yucca Mountain. Proceedings of the 8th International Conference on High Level Radioactive Waste Management, pp. 16–23.

Byers Jr., F.M., Carr, W.J., Orkild, P.P., Quinlivan, W.D., Sargeant, K.A., 1976. Volcanic suites and related cauldrons of the Timber Mountain–Oasis Valley Caldera Complex. United States Geological Survey Professional Paper 919.

Carr, W.J., 1990. Styles of extension in the Nevada test site region, Southern Walker Lane Belt: an integrated volcano-tectonic and detachment fault model. Geological Society of America Memoir 176, 283–303.

Childs, C., Watterson, J., Walsh, J.J., 1995. Fault overlap zones within

developing normal fault systems. Journal of the Geological Society of London 152, 535–549.

Connor, C.B., Hill, B.E., 1995. Three nonhomogeneous Poisson models for the probability of basaltic volcanism: application to the Yucca Mountain region, Nevada. Journal of Geophysical Research 94, 10, 107–10,125.

Connor, C.B., Stamatakos, J.A., Ferrill, D.A., Hill, B.E., Ofoegbu, G.I., Conway, F.M., Sagar, B., Trapp, J., 2000. Geologic factors controlling patterns of small-volume basaltic volcanism: application to a volcanic hazard assessment at Yucca Mountain, Nevada. Journal of Geophysical Research 105, 407–432.

CRWMS M&O (Civilian Radioactive Waste Management System Management and Operating Contractor), 1998. Geology of The Exploratory Studies Facility Topopah Spring Loop. BAB 000000-01717-0200-00002, REV 01. U.S. Department of Energy, Las Vegas, Nevada.

CRWMS M&O (Civilian Radioactive Waste Management System Management and Operating Contractor), 2000a. Fracture Geometry Analysis for the Stratigraphic Units of the Repository Host Horizon. Analysis model report. ANL-EBS-GE-000006 REV 00. U.S. Department of Energy, Las Vegas, Nevada.

CRWMS M&O (Civilian Radioactive Waste Management System Management and Operating Contractor), 2000b. Geologic Framework Model (GFM 3.1). Analysis model report. MDL-NBS-GS-000002 Rev 00 ICN 01. U.S. Department of Energy, Las Vegas, Nevada. CRWMS M&O, ACC: MOL. 20000121.0115.

CRWMS M&O (Civilian Radioactive Waste Management System Management and Operating Contractor), 2001. Yucca Mountain Science and Engineering Report. DOE/RW-0539. U.S. Department of Energy, Las Vegas, Nevada.

Dawers, N.H., Anders, M.H., 1995. Displacement–length scaling and fault linkage. Journal of Structural Geology 17, 607–614.

Day, W.C., Dickerson, R.P., Potter, C.J., Sweetkind, D.S., San Juan, C.A., Drake II, R.M., Fridrich, C.J., 1998a. Bedrock geologic map of the Yucca Mountain area, Nye County, Nevada. U.S. Geological Survey Miscellaneous Investigations Series Map I-2627, scale 1:24,000.

Day, W.C., Potter, C.J., Sweetkind, D.S., Dickerson, R.P., San Juan, C.A., 1998b. Bedrock geologic map of the Central Block Area, Yucca Mountain, Nye County, Nevada. U.S. Geological Survey Miscellaneous Investigations Series Map I-2601, scale 1:6000.

Dunne, W.M., Ferrill, D.A., Crider, J.G., Hill, B.E., Waiting, D.J., La Femina, P.C., Morris, A.P., Fedors, R.W., 2003. Orthogonal jointing during coeval igneous degassing and normal faulting, Yucca Mountain, Nevada. Geological Society of America Bulletin 115, 1492–1509.

Ferrill, D.A., Morris, A.P., 2001. Displacement gradient and deformation in normal fault systems. Journal of Structural Geology 23, 619–638.

Ferrill, D.A., Stamatakos, J.A., Jones, S.M., Rahe, B., McKague, H.L., Martin, R.H., Morris, A.P., 1996a. Quaternary slip history of the Bare Mountain fault (Nevada) from the morphology and distribution of alluvial fan deposits. Geology 24, 559–562.

Ferrill, D.A., Stirewalt, G.L., Henderson, D.B., Stamatakos, J.A., Spivey, K.H., Wernicke, B.P., 1996b. Faulting in the Yucca Mountain Region, Critical Review and Analyses of Tectonic Data from the Central Basin and Range. NUREG/CR-6401. U.S. Nuclear Regulatory Commission, Washington, DC.

Ferrill, D.A., Stamatakos, J.A., Sims, D., 1999a. Normal fault corrugation: implications for growth and seismicity of active normal faults. Journal of Structural Geology 21, 1027–1038.

Ferrill, D.A., Winterle, J., Wittmeyer, G., Sims, D., Colton, S., Armstrong, A., Morris, A.P., 1999b. Stressed rock strains groundwater at Yucca Mountain, Nevada. GSA Today 9(5), 1–8.

Fridrich, C.J., 1999. Tectonic evolution of the Crater Flat basin, Yucca Mountain region, Nevada. In: Wright, L., Troxel, B. (Eds.), Cenozoic Basins of the Death Valley Region. Geological Society of America Special Paper 333, pp. 169–196.

Harmsen, S.C., 1994. The Little Skull Mountain, Nevada, earthquake of 29 June 1992: aftershock focal mechanisms and tectonic stress field implications. Bulletin of the Seismological Society of America 84, 1484–1505.

Hoek, E., Brown, E.T., 1988. The Hoek–Brown failure criterion—a 1988 update. 15th Canadian Rock Mechanics Symposium, pp. 31–38.

Huggins, P., Watterson, J., Walsh, J.J., Childs, C., 1995. Relay zone geometry and displacement transfer between normal faults recorded in coal-mine plans. Journal of Structural Geology 17, 1741–1755.

Mandl, G., 1988. Mechanics of Tectonic Faulting, Elsevier, New York.

Mongano, G.S., Singleton, W.L., Moyer, T.C., Beason, S.C., Eatman, G.L.W., Albin, A.L., Lung, R.C., 1999. Geology of the Enhanced Characterization of the Repository Block Cross Drift—Exploratory Studies Facility, Yucca Mountain Project, Yucca Mountain, Nevada, Bureau of Reclamation and U.S. Geological Survey, Denver, CO.

Morris, A.P., Ferrill, D.A., Henderson, D.B., 1996. Slip tendency analysis and fault reactivation. Geology 24, 275–278.

Oldow, J.S., 1992. Late Cenozoic displacement partitioning in the northwestern Great Basin. Geological Society of Nevada, Proceedings Volume, Walker Lane Symposium, Structure, Tectonics & Mineralization of the Walker Lane, pp. 17–52.

Peacock, D.C.P., Sanderson, D.J., 1994. Geometry and development of relay ramps in normal fault systems. American Association of Petroleum Geologists Bulletin 78, 147–165.

Potter, C.J., Dickerson, R.P., Sweetkind, D.S., Drake II, R.M., Taylor, E.M., Fridrich, C.J., San Juan, C.A., Day, W.C., 2002. Geologic map of the Yucca Mountain region, Nye County, Nevada: U.S. Geological Survey Miscellaneous Geologic Investigations Series Map I-2755, scale 1:50,000, 37pp. pamphlet.

Sawyer, D.R., Fleck, R.J., Lanphere, M.A., Warren, R.G., Broxton, D.E., Hudson, M.R., 1994. Episodic caldera volcanism in the Miocene southwestern Nevada volcanic field: revised stratigraphic framework, $^{40}Ar/^{39}Ar$ geochronology, and implications for magmatism and extension. Geological Society of America Bulletin 106, 1304–1318.

Scott, R.B., Bonk, J., 1984. Preliminary geologic map of Yucca Mountain, Nye County, Nevada with Geologics. U.S. Geological Survey Open-File Report 84-494.

Simonds, W.F., Whitney, J.W., Fox, K., Ramelli, A., Yount, J.C., Carr, M.D., Menges, C.D., Dickerson, R., Scott, R.B., 1995. Map of fault activity of the Yucca Mountain area, Nye County, Nevada. U.S. Geological Survey Miscellaneous Investigations Series Map I-2520, scale 1:24,000.

Sims, D.W., Morris, A.P., Ferrill, D.A., Sorkhabi, R., 2004. Extensional fault systems evolution and reservoir connectivity. American Association of Petroleum Geologists Memoir: Faults, Fluid Flow, and Petroleum Traps, in press.

Snow, J.K., Wernicke, B.P., 2000. Cenozoic tectonism in the central Basin and Range: magnitude, rate, and distribution of upper crustal strain. American Journal of Science 300, 659–719.

Stock, J.M., Healy, J.H., 1988. Stress field at Yucca Mountain, Nevada, geologic and hydrologic investigations of a potential nuclear waste disposal site at Yucca Mountain, southern Nevada. In: Carr, M.D., Yount, J.C. (Eds.), U.S. Geological Survey Bulletin 1790, pp. 87–94.

Stock, J.M., Healy, J.H., Hickman, S.H., Zoback, M.D., 1985. Hydraulic fracturing stress measurements at Yucca Mountain, Nevada, and relationship to regional stress field. Journal of Geophysical Research 90, 8691–8706.

Sweetkind, D.S., Anna, L.O., Williams-Stroud, S.C., Coe, J.A., 1997. Characterizing the fracture network at Yucca Mountain, Nevada, Part 1: integration of field data for numerical simulations, fractured reservoirs. In: Hoak, T.E., Blomquist, P.K., Klawitter, A. (Eds.), Characterization and Modeling Guidebook—1997. Rocky Mountain, Denver, CO. Association of Geologists, pp. 185–196.

Sweetkind, D.S., Beason, S.C., Buesch, D.C., 2004. Overview of the stratigraphic and structural setting of Yucca Mountain, Nevada, USA. International Journal of Rock Mechanics, in press.

Trudgill, B., Cartwright, J., 1994. Relay-ramp forms and normal-fault linkages, Canyonlands National Park, Utah. Geological Society of America Bulletin 106, 1143–1157.

Twiss, R.J., Moores, E.M., 1992. Structural Geology, W.H. Freeman and Company, New York.

U.S. Department of Energy, 1998. Viability assessment of a repository at Yucca Mountain, Volume 3: total system performance assessment, DOE/RW-0508/V3, December 1998.

U.S. Geological Survey, 1999. North America shaded relief map, editorial. U.S. Geological Survey, EROS Data Center, Reston, Virginia, http://nationalatlas.gov/atlasftp.html. filename: shdrfi0201.tar.92.

Walsh, J.J., Watterson, J., 1991. Geometric and kinematic coherence and scale effects in normal fault systems. In: Roberts, A.M., Yielding, G., Freeman, B. (Eds.), The Geometry of Normal Faults. Geological Society of London Special Publication 56, pp 193–203.

Walsh, J.J., Bailey, W.R., Childs, C., Nicol, A., Bonson, C.G., 2003. Formation of segmented normal faults: a 3D perspective. Journal of Structural Geology 25, 1251–1262.

Willemse, E.J.M., Pollard, D.D., Aydin, A., 1996. Three-dimensional analyses of slip distributions on normal fault arrays with consequences for fault scaling. Journal of Structural Geology 18, 295–309.

Young, S.R., Morris, A.P., Stirewalt, G.L., 1992a. Preliminary structural interpretation of reflection seismic line AV-1. CNWRA 92-024. CNWRA, San Antonio, TX.

Young, S.R., Stirewalt, G.L., Morris, A.P., 1992b. Geometric models of faulting at Yucca Mountain. CNWRA 92-008. CNWRA, San Antonio, TX.

Zoback, M.L., Anderson, R.E., Thompson, G.A., 1981. Cainozoic evolution of the state of stress and style of tectonism of the Basin and Range province of the western United States. Philosophical Transactions of the Royal Society of London A300, 407–434.